Advances on photoconductive InAs/GaSb type-II superlattice long-wavelength infrared detectors for high operating temperature

Raphael Müller *[a], Jasmin Niemasz[a], Volker Daumer[a], Andrzej Janaszek[b], Jarosław Jureńczyk[b], Robert Rehm[a]
[a]Fraunhofer Institute for Applied Solid State Physics (IAF), Tullastr. 72, 79108 Freiburg (Germany);
[b]Vigo System S.A., 129/133 Poznanska Str., 05-850 Ozarow Mazowiecki (Poland)

ABSTRACT

The fabrication and characterization of InAs/GaSb type-II superlattice long-wavelength infrared (LWIR) photodetectors for high operating temperature (HOT) are assessed regarding possible device yield. We investigate laterally-operated photoconductors with a detector cutoff wavelength in the LWIR at an operating temperature accessible with 3-stage thermoelectric cooling, realized by suitably tailoring the layer composition. Type-II superlattices with a layer composition of 14 monolayers InAs and 7 monolayers GaSb are grown on semi-insulating 3-inch GaAs substrates. We report on the growth of three different buffer layer variants that serve as growth templates for GaSb-based layers on GaAs substrates. The characterization of 75 nominally equal single element detectors per sample evidences the reliability of device processing. The electro-optical evaluation of a randomly chosen subset indicates a high uniformity of responsivity and noise of LWIR InAs/GaSb HOT photoconductors. At 210 K, the devices operate at a cutoff wavelength of 10.5 µm and achieve a mean peak spectral detectivity of 3.3 x 10^8 Jones.

Keywords: HOT, TEC, InAs/GaSb, T2SL, photoconductor, immersion, infrared detector, LWIR

1. INTRODUCTION

Fast and sensitive detection of radiation in the longwave infrared (LWIR, 8-12 µm) is essential for numerous applications in science and industry which can only be realized with photonic detectors. Furthermore, small size and low cost of detection systems are required for widespread distribution. Hence, cooling requirements for operation need to be compatible with thermoelectric cooling. In this field of operation at high operating temperature (HOT, 180 K – 300 K) detector concepts that use Mercury Cadmium Telluride (MCT) are state-of-the-art. However, the use of Mercury and Cadmium is threatened by the European Restriction of Hazardous Substances (RoHS), which motivates the investigation of alternative material systems for infrared HOT detection. Besides HOT, MCT is the prevalent material system also for cryogenically-cooled operation. However, here detectors fabricated from InAs/GaSb type-II superlattices (T2SLs) have emerged as a III-V alternative since the proposal of Smith and Mailhiot in 1987 [1]. Accordingly, a recent research trend aims at the development of unrestricted T2SL-based HOT detector concepts [2,3,4]. Latest results show that laterally-operated HOT T2SL photoconductors can approach or even outperform MCT-based devices [3,5].

The detector concept that is elaborated on in this paper is a laterally-operated photoconductor fabricated with InAs/GaSb T2SLs. It has a cutoff wavelength in the LWIR at an operating temperature that is accessible with a thermo-electric cooler (TEC) assembly. The key figure of merit for assessment of device performance is the spectral detectivity $D^*(\lambda)$ that connects photosignal and noise, in particular the spectral responsivity $R(\lambda)$ to the noise current I_n:

$$D^*(\lambda) = \frac{R(\lambda)}{I_n}\sqrt{A_o\,\Delta f}$$

It is normalized by the square root of the apparent optical area A_o and the bandwidth Δf, respectively. Hence, $D^*(\lambda)$ can be improved by increasing the apparent optical area via employing microlens technology. A microlens, that focuses incoming radiation onto the photosensitive detector area, is preferably immersed directly into the substrate material of a backside illuminated detector. Evidently, this requires a transmissive substrate, which is provided for semi-insulating GaAs. This substrate material is commercially available at low cost and enables upscaling the growth to larger substrate diameters. However, the lattice constant of GaAs differs by 7.8% from the lattice constant of GaSb, which is the native, lattice-matched substrate for conventional InAs/GaSb T2SLs. This lattice mismatch enforces the growth of a buffer layer.

Optical Components and Materials XVI, edited by Shibin Jiang, Michel J. F. Digonnet, Proc. of SPIE Vol. 10914, 1091416 · © The Authors. Published under a Creative Commons Attribution CC-BY 3.0 License
doi: 10.1117/12.2506624

For the T2SL devices in this paper a linearly graded metamorphic buffer layer is employed as will be discussed later on. This buffer layer serves as growth template for the layers deposited on top from which electro-optical devices are fabricated. Defects on the surface on this template deteriorate the crystal structure of the layers above which can ultimately lead to device deterioration or failure. Hence, a smooth growth template with a low surface defect density is required to reach a high device yield which is a decisive figure of merit for cost-effective detector fabrication. To improve the quality of the growth template, we investigate the impact of an intermediate GaSb buffer layer of different width on top of the metamorphic buffer. It is implemented to enhance the surface quality and further stabilize the lattice constant.

In the following, we investigate how uniform the detector properties of our LWIR HOT photoconductor are and assess the areal homogeneity. We begin by describing the growth of three superlattice samples on different buffer layers and the processing sequence for device fabrication. Afterwards 75 devices per sample are electrically characterized and the areal distribution of the dark-current of these devices is discussed. Thereupon, the electro-optical characterization data of a smaller number of randomly chosen devices is reported on.

2. DETECTOR FABRICATION

2.1 Sample growth

Three superlattice samples are grown on 1100 µm thick, semi-insulating 3-inch GaAs(001) wafers by molecular beam epitaxy. In Figure 1a the full layer stack is presented. Two buffer layers are grown on top of the GaAs substrate to compensate the strain between the GaAs substrate and the GaSb-based superlattice above. First, a metamorphic buffer layer is grown at 450°C. In this layer As is gradually substituted by Sb over a distance of 2 µm whereby the lattice constant is increased accordingly. On top, an intermediate GaSb buffer layer is grown. This buffer layer differs in width t_{IBL} for the three samples A (t_{IBL} = 0.1 µm), B (t_{IBL} = 1 µm) and C (t_{IBL} = 10 µm). This results in three growth templates for superlattice deposition. The nominally equal non-intentionally doped superlattices on top have a layer composition of 14 monolayers (ML) InAs and 7 ML GaSb and comprise 750 periods. In the end, a heavily n-doped T2SL contact layer terminates the growth structure.

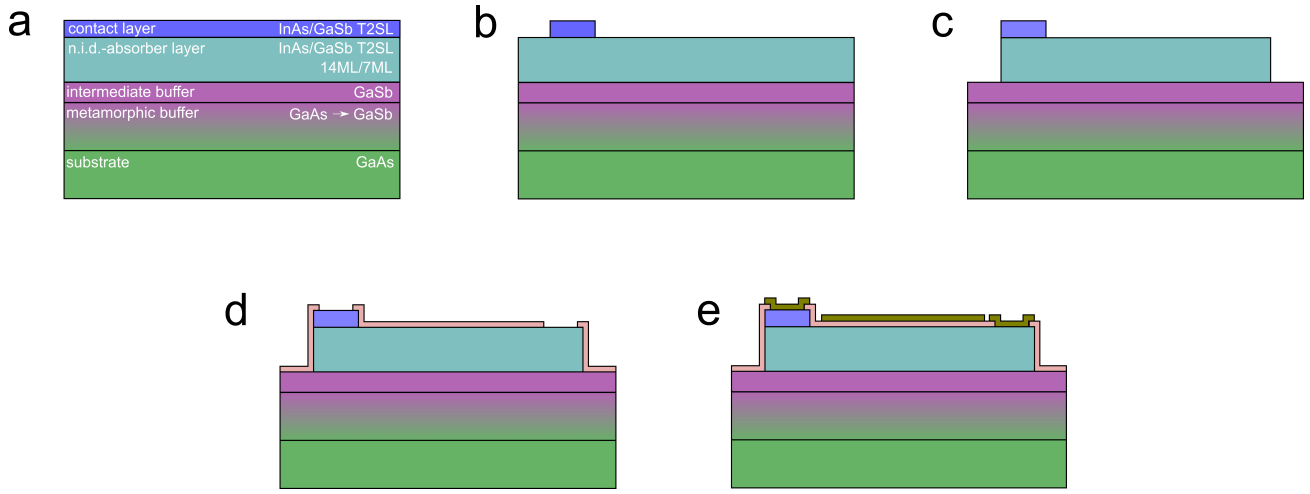

Figure 1: Schematic T2SL layer structure (a) and processing steps for the fabrication of laterally-operated photoconductor devices on GaAs substrate. Structuring of the contact layer (b) and absorber layer via ICP etching (c), dielectric passivation and passivation opening (d), metallization (e). This processing sequence yields an asymmetric device that was designed to investigate sweep-out suppression.

2.2 Device processing

Fraunhofer IAF has a long track record in research and development of high-performance infrared detectors and detector arrays for cryogenically cooled operation. This processing know-how is employed to fabricate laterally-operated HOT photoconductors. The processing sequence, which is described below, yields quadratic photoconductor elements of various edge length. The metal contacts that connect the detector to the external circuit are located on two opposing edges and extend over its entire width.

The processing sequence described in Figure 1 is equal for all three samples. First, the T2SL n-type contact layer is defined by dry-etching, using an inductively coupled plasma (ICP) technique (b). Then the photosensitive T2SL absorber layer is mesa-structured in yet another dry-etching step (c). Furthermore, a dielectric passivation is applied on the entire wafer surface and afterwards selectively opened in the designated contact area (d). Then a Ti/Au/Pt/Au metal sequence is evaporated on top, serving as a contact metallization in the contact area and as a front-side mirror that allows for double pass of backside incident radiation in the absorber region (e).

Further processing steps are performed at VIGO System and comprise dicing into single devices and mounting to TEC. For this, detector material is provided to VIGO in chips with 15 x 15 single detector elements (see Figure 2). The pitch between individual elements is 1480 µm vertical and horizontal direction. This spacing enables the immersion of hyperhemisperic concentrator lenses into the substrate, which is a standardized process at VIGO for increase of detectivity. Therefore, a 3-inch wafer can feature four of such chips and some extra device structures on the edges, resulting in approximately 1000 usable single detector elements that can be processed per 3-inch wafer. The wafer chip in Figure 2 comprises 3 x 75 quadratic detector elements with an edge length of 30 µm, 50 µm and 100 µm, respectively.

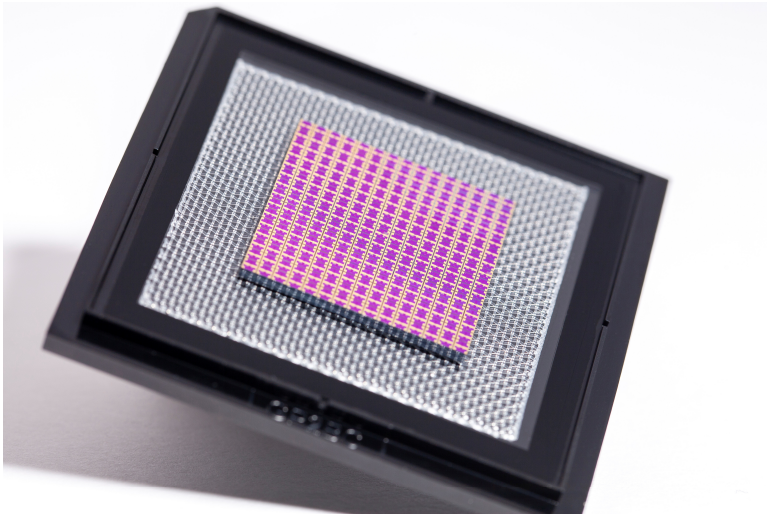

Figure 2: GaAs-based chip comprising 15 x 15 laterally-operated LWIR InAs/GaSb T2SL HOT single elements photoconductors. The device pitch is 1480 µm, both in horizontal and vertical direction.

The processing sequence presented above yields asymmetric devices. In the first mesa etch step (see Figure 1b) a single-sided contact layer is formed that remains only on the left. In fact, this device design is part of a design study in which we investigated single-sided, double-sided and no contact layers at all for laterally-operated photoconductor devices. This design study was motivated by the history of MCT photoconductor developments, in which introducing doping or heterojunction layers in the contact region has led to the suppression of sweep-out effects that resulted in a significant increase of the responsivity [6, 7, 8]. In our study that focused on the TEC-accessible temperature range, we did not observe sweep-out suppression for any contact layer option (single-sided, double-sided, none) on any of the three samples. Probably, this relates to the carrier lifetime in LWIR T2SLs being too short for such contact related effects to be observed. In fact, the only impact observed for the different contact layer options was an improved contact resistance when a contact layer was present. This explains our asymmetric device layout. From here on, all data was acquired on devices with a single-sided contact layer.

3. ELECTRO-OPTICAL CHARACTERIZATION

3.1 Batch characterization

From a commercial standpoint device yield is a decisive figure of merit. We started to assess it by characterizing all 100 x 100 μm^2 devices from a wafer chip as the one presented in Figure 2. As this wafer chip comprises detectors with 30 µm, 50 µm and 100 µm edge length, this results in the characterization of 5 x 15 devices. The measurements were performed with our semiautomatic wafer prober from Cascade Microtech that was modified to fit characterization needs for T2SL mesa detectors [9]. This setup enables full-wafer electro-optical testing at temperatures ranging from liquid nitrogen to room temperature. After initial alignment and positioning, a predefined wafer area can automatically be mapped with a probe card. The probe card employed here enables the simultaneous characterization of three devices positioned next to each other.

In Figure 3 the current-voltage characterization of all 75 devices with a 100 x 100 μm^2 absorber mesa at 200 K is presented for samples A, B and C. On the left we present the differential resistance for all 75 devices at bias voltages between 0 V and 1 V. The distribution and scatter amongst the devices is illustrated by the 25% - 75% range, the 10% - 90% range, the median and the mean values. At low bias voltage the differential resistance is constant, indicating a perfectly linear current-voltage dependence. Towards higher bias voltage a minor decrease is observed for devices from all samples. Comparison of devices from different samples evidences a decline in the differential resistance from sample A to sample C. For the mean value, at a typical operating bias of 0.2 V for such a device, this amounts to 60.7 Ω (A), 51.9 Ω (B) and 40.1 Ω (C), respectively. Since this trend in differential resistance from sample A to C coincides with an increase in thickness of the GaSb-based intermediate buffer layer, it suggests a shunt contribution from this buffer layer. Besides absolute value the differential resistances also differ in width of the distribution. The standard deviation of the differential resistance for sample C at 0.2 V is lower in absolute terms (2.6 Ω) and relative to the mean value (6.5%) than the respective values for samples A and B. This superior homogeneity can either be attributed to an overall better areal homogeneity, possibly due to the increased thickness of the intermediate buffer layer, or possible directional trends for samples A and B that remained unidentified in the analysis up to this point.

On the right of Figure 3 color-coded maps present the areal distribution of the respective dark-current at a bias value of 0.2 V for samples A, B and C. Each single element detector is represented by one color-coded pixel. No trend related to the 1 x 3 probe card pattern is observed for either of the color-coded maps. Hence, it can be assumed that the characterization of each device is independent of the respective needles of the probe card connected to it. So the presented values can be attributed directly to the individual devices. The mean values of the dark-current are 3.30 mA (A), 3.86 mA (B) and 5.00 mA (C), the respective standard deviations are 0.28 mA (A), 0.36 mA (B) and 0.31 mA (C). For better comparability the values are presented in Table 1 alongside the ratio of standard deviation and mean value of the dark-current. Looking at the respective color distribution, apparently for none of the samples an unambiguous directional trend across the wafer area can be observed. However, for all samples there are regions in which the device dark-current is larger than in others. These differences need to be assigned to inhomogeneities caused by the growth or the processing sequence. The narrower distribution of the differential resistance in sample C, that was discussed before, can hence be related to superior areal homogeneity and is not due to previously unidentified trends.

This analysis of dark-current measured for a larger number of devices already highlights the importance of a suitable buffer layer for growth of InAs/GaSb T2SLs on GaAs. Devices from sample A show a lower device dark-current, which might be related to an additional shunt contribution for samples B and C and, hence, favors the absence of an intermediate buffer layer. Measurement results of the dark-current for devices from sample C show a better areal homogeneity that is achieved with a thick intermediate buffer layer. Currently we do not know whether the narrower distribution in dark-current for devices from sample C is a result of a predominant shunt or enabled by a superior growth template due to the thicker buffer layer. Evidently, a combination of a small shunt at good areal homogeneity of the device dark-current is preferred. The improved understanding of the buffer related effect and the means to properly suppress it are subject of the current development. Irrespective of absolute values and the distribution and the dark-current for devices from samples A, B and C, all 75 single element devices from each sample show a similar, close to ohmic current-voltage dependence at 200 K. No directional trend concerning the dark-current values is observed for the investigated wafers. This supports the reliability of the growth and processing sequence and prospects a high device fabrication yield.

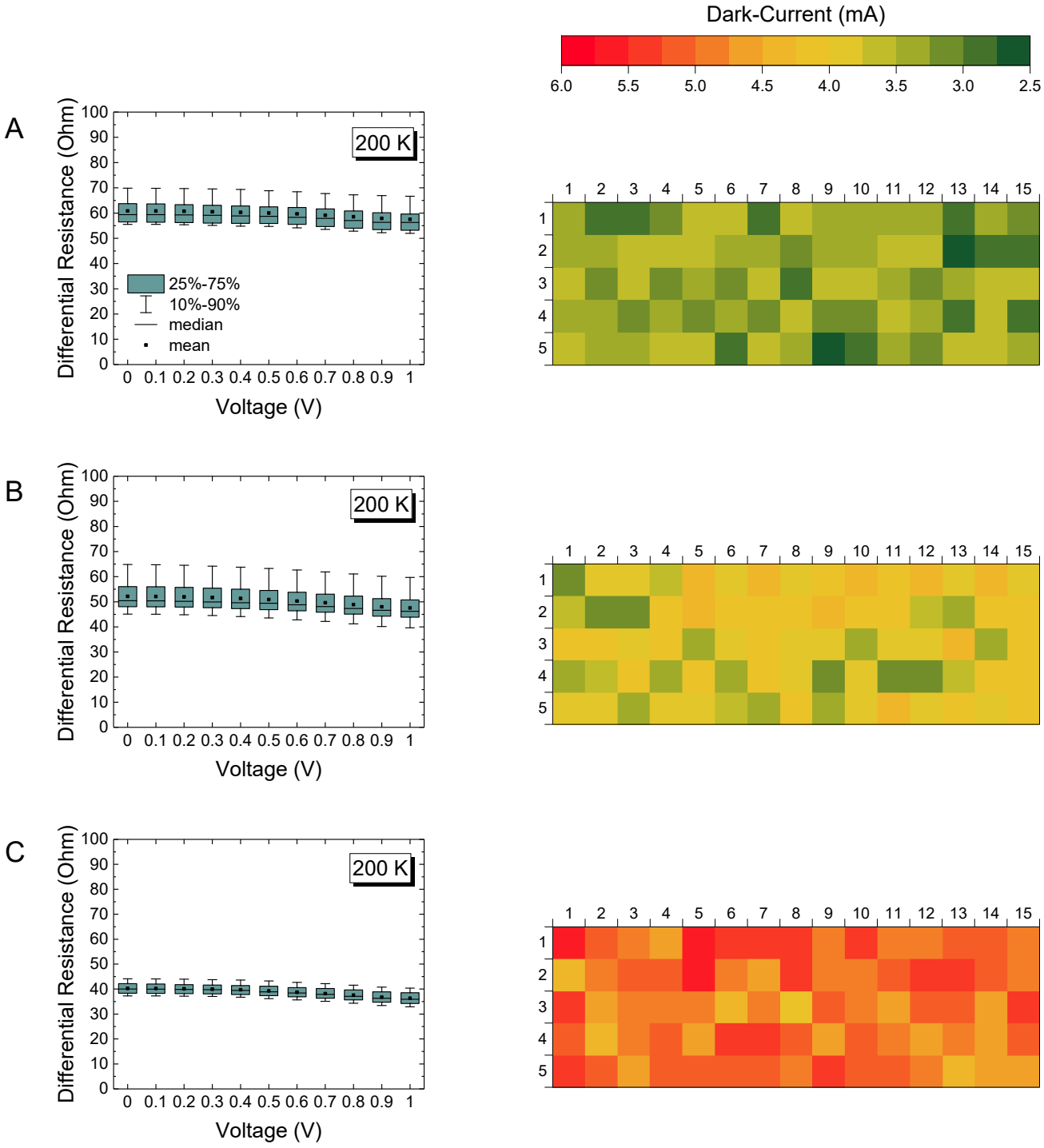

Figure 3: Current-voltage characterization of 75 quadratic photoconductor devices with 100 µm edge length for samples A, B and C at 200 K. In the left the differential resistance is shown at different bias voltages in box plots. On the right the respective color coded maps of the device dark-current at an operating bias of 0.2 V are presented.

Table 1: Thickness of the intermediate buffer layer t_{IBL}, mean value of the differential resistance $R_{diff,mean}$ and the dark-current $I_{dark,mean}$ as well as the standard deviation of the dark-current σ_I and the ratio $\sigma_I/I_{dark,mean}$ for 75 devices from samples A, B and C characterized at 200 K and 0.2 V.

Sample	t_{IBL} (µm)	$R_{diff,mean}$ (Ω)	$I_{dark,mean}$ (mA)	σ_I (mA)	$\sigma_I/I_{dark,mean}$
A	0.1	61.0	3.33	0.28	8.6%
B	1	51.9	3.86	0.36	9.4%
C	10	40.1	5.00	0.31	6.2%

3.2 Electro-optical characterization under backside-illumination

Wafer chips comprising 225 front-side metallized detector structures were provided to VIGO System for dicing into single devices and mounting the detector elements onto thermo-electric coolers. These processes are lengthy, costly and labor-intensive. We exemplify the assessment by presenting characterization data of a subset of 10 devices from sample C that was assembled to TEC and characterized electro-optically. The devices were chosen randomly over the entire wafer range and were characterized by spectral photoresponse at 0.2 V and 210 K, an operating temperature accessible with 3-stage thermoelectric cooling. The spectra were corrected after additional characterization on a black-body setup. Due to the small detector area a measurement uncertainty of 10% in responsivity is assumed. Furthermore, noise spectra were obtained at the same operating bias and temperature.

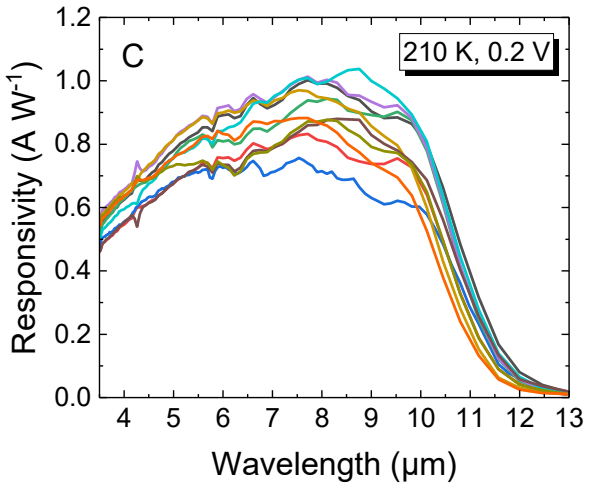

Figure 4: Current responsivity of 10 randomly chosen 100 x 100 µm^2 laterally-operated photoconductors from sample C under backside-illumination at 210 K and 0.2 V.

In Figure 4 the measured current responsivity is presented for all assembled devices. The photoresponse curves exhibit similar spectral shapes and show a mean 50% cutoff wavelength of 10.5 µm with a standard deviation of 0.1 µm. The mean peak spectral responsivity is 0.92 A/W. The standard deviation of this figure of merit is smaller than the measurement uncertainty. So a prolonged discussion of the responsivity values is omitted and it can be stated that a uniform spectral responsivity is observed across the wafer in this study.

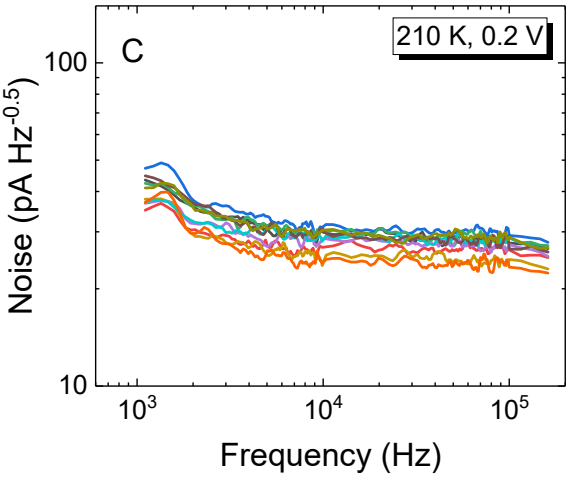

Figure 5: Noise spectral density of 10 randomly chosen 100 x 100 µm^2 laterally-operated photoconductors from sample C under backside-illumination at 210 K and 0.2 V.

In Figure 5 the noise spectral density of the 10 devices under test is presented between 1.1 kHz and 100 kHz. Once more similar trends and noise levels are observed for all detectors. At low frequencies a small, yet dominating 1/f-noise contribution is observed up to a knee frequency around 10 kHz. At higher frequencies, for all devices an almost white noise level is found. The mean noise spectral density between 10 kHz and 100 kHz is around 28 pA Hz$^{-1/2}$. In an earlier publication temperature-dependent characterization of a single photoconductor device from this sample suggested g-r-noise limited operation [5], which we also assign to the samples discussed here.

In conclusion, we observe narrow distributions and uniform properties of responsivity and noise for 10 randomly chosen devices from sample C. This suggests that the measured devices properties are representative of the sample. Hence, the prospect of a high device yield in section 3.1, that was exclusively based on current-voltage data, is affirmed by the characterization of responsivity and noise. A meaningful assessment of uniformity and homogeneity across the entire wafer based on characterization of 10 randomly chosen devices, that were distributed over a smaller wafer area, is impossible. However, considering that so far no device failures or directional trends on the wafer were observed, the extrapolation of our findings to the entire wafer would result in the aforementioned approximately 1000 usable detector devices per 3-inch wafer. The responsivity and noise obtained at 210 K result in mean values of the peak spectral detectivity of 3.3 x 10^8 Jones and the spectral detectivity of 1.6 x 10^8 Jones at 10.6 µm for non-immersed devices, which is less than a factor of 2 from guaranteed values of comparable, commercially available VIGO MCT photoconductors cooled to 210 K with a 3-stage TEC. Furthermore, the device performance of the LWIR InAs/GaSb T2SL HOT photoconductors is expected to increase after doping optimization of the so far non-intentionally doped absorber superlattice which makes it even more competitive. Like for MCT-based photodetectors, the spectral detectivity can be increased further via immersion of a hyperhemispheric concentrator lens into the GaAs substrate for T2SL-based photoconductors, which is a standardized back-end processing step at VIGO.

4. SUMMARY

In this paper, we assess the device yield for LWIR InAs/GaSb T2SL HOT photoconductors grown on semi-insulating 3-inch GaAs substrates. Three buffer layer variants are motivated that allow for lattice-matched growth of non-intentionally doped T2SL superlattices with a 14 ML/7 ML InAs/GaSb layer composition on GaAs. The layer growth and the processing sequence for the fabrication of laterally-operated photoconductors are presented. Current-voltage characterization of 75 nominally equal detector elements per superlattice sample at 200 K evidences uniform characteristics for devices from each sample. For devices from different samples a systematically reduced device resistance is found for increased thickness of a GaSb-based buffer layer which suggests a shunt contribution from this buffer layer. A subset of 10 randomly chosen detector elements from one sample is assembled and characterized at an operating temperature of 210 K. The spectral

photoresponse and the noise spectral density show a cutoff wavelength of 10.5 μm and a mean peak spectral detectivity of 3.3 x 10^8 Jones at a good homogeneity across the wafer area under study. The high processing and fabrication yield suggests that approximately 1000 single element detectors can be fabricated per 3-inch wafer with a spacious distribution that allows for subsequent immersion of hyperhemispheric concentrator lenses into the substrate. Additionally, the spectral detectivity is expected to increase due to optimized doping of the up to now non-intentionally doped absorber superlattice.

Acknowledgements: Project funding through the Horizon 2020 Research and Innovation programme under grant agreement No.688265 is gratefully acknowledged.

REFERENCES

[1] Smith, D. L., Mailhiot, C., "Proposal for strained type II superlattice infrared detectors," J. Appl. Phys. 62, 2545-2548 (1987)
[2] Benyahia, D., Kubiszyn, Ł.., Michalczewski, K., Boguski, J., Kębłowski, A., Martyniuk, P., Piotrowski, J. and Rogalski, A., "Electrical Properties of Midwave and Longwave InAs/GaSb Superlattices Grown on GaAs Substrates by Molecular Beam Epitaxy", Nanoscale Research Letters, 13:196 (2018)
[3] Michalczewski, K., Kubiszyn, Ł., Martyniuk, P., Wu, C.H., Jureńczyk, J., Grodecki, K., Benyahia, D., Rogalski, A. and Piotrowski, J., "Demonstration of HOT LWIR T2SLs InAs/InAsSb photodetectors grown on GaAs substrate", Infrared Physics & Technology 95, 222-226 (2018)
[4] Martyniuk, P., Benyahia, D., Kowalewski, A., Kubiszyn, Ł., Stepien, D., Gawron, W., and Rogalski, A., "Mid-wave T2SLs InAs/GaSb single pixel PIN detector with GaAs immersion lens for HOT condition", Solid-State Electronics 119, 1-4 (2016)
[5] Müller, R., Gramich, V., Wauro, M., Niemasz, J., Kirste, L., Daumer, V., Janaszek, A., Jureńczyk, J. and Rehm, R., "High operating temperature InAs/GaSb type-II superlattice detectors on GaAs substrate for the long wavelength infrared", Infrared Physics & Technology 96, 141-144 (2019)
[6] Shacham-Diamand, Y.J., and Kidron, I., "Contact and bulk effects in intrinsic photoconductive infrared detectors", Infrared Physics 21(2), 105-115 (1981)
[7] Smith, D.L., Arch, D.K., Wood, R.A., and Scott, M.W., "HgCdTe heterojunction contact photoconductor", Appl. Phys. Lett. 45(1), 83-85 (1984)
[8] Smith, D.L., "Effects of blocking contacts on generation-recombination noise and responsivity in intrinsic photoconductors", Journal of Applied Physics 56 (6), 1663 (1984)
[9] Wörl, A., Daumer, V., Hugger, T., Kohn, N., Luppold, W., Müller, R., Niemasz, J., Rehm, R., Rutz, F., Schmidt, J., Schmitz, J., Stadelmann, T., Wauro, M., "Advances in the Characterization of InAs/GaSb Superlattice Infrared Photodetectors", Proc. Of SPIE 9987, 99870U 1-7 (2016)